Silver Nanoneedle Probes Enable Sustained DC Current, Single-Channel Resistive Pulse Nanopore Sensing

Essraa A. Hussein[§] and Ryan J. White[§‡]*

[§] Department of Chemistry, University of Cincinnati, Cincinnati, OH 45221

[‡] Department of Electrical Engineering and Computer Science, University of Cincinnati, Cincinnati, OH 45221

ABSTRACT

Resistive pulse sensing using ion channel proteins (biological nanopores) has been evolving as a single-molecule approach to detect small biomolecules owing to the atomically-precise pore size reproducibility, high signal-to-noise ratio, and molecular selectivity. The incorporation of biological nanopores in sensing platforms requires a stable lipid membrane that can be formed by a variety of methods such as the painting method and droplet-based techniques. However, these methods are limited by the fragility of the unsupported bilayer or the need for specific microdevices. Electrode-supported bilayers, in which a metal electrode is used as a support structure, have been recently developed using a fine gold nanoneedle. We previously described the utility of the gold nanoneedle-supported ion channel probe to detect small molecules with high spatial resolution, however, it exhibited a channel current decay over time, which affected the binding frequency of the target molecule to the protein pore as well. Here, we introduce a silver nanoneedle probe to support lipid bilayer formation and ion channel measurements. The silver nanoneedle mitigates the current decay observed on gold electrodes and produces stable DC channel currents. Our findings propose the formation of a AgCl layer creating a non-polarizable electrode. The new nanoneedle is successfully applied for single-molecule detection of sulfonated β-cyclodextrin (S_7βCD) using αHL as a test bed protein. We believe that this new silver nanoneedle platform has great potential given the relative ease of lipid bilayer formation and stable open channel currents.

* *Corresponding Author; ryan.white@uc.edu*

INTRODUCTION

Resistive pulse sensing is a sensing technique that relies on the measurement of the transient blocking current caused by single molecules entering or passing through a micro- or nanoscale orifice or pore.[1–3] Nanopore-based techniques, using a biological or solid-state nanopore, have been widely applied in the detection of biomolecules such as DNA,[4,5] miRNA,[6–8] neurotransmitters,[9–11] peptides,[12] and proteins,[13,14] in addition to the functionality of these techniques for DNA sequencing.[15,16] Nanopore, resistive-pulse techniques provide single particle-to-particle readout capabilities, high sensitivity, temporal resolution, signal-to-noise, and molecular selectivity.[1–3,15,17–20] Biological nanopores, or ion channel proteins, have attracted more interest in nanopore sensing and molecular flux imaging applications due to the atomic-level precision of the pore size.[21,22] To perform resistive pulse detection with a biological nanopore, typically the protein pore is reconstituted in a lipid membrane suspended between two electrolyte compartments when a potential is applied across the membrane. When a specific analyte binds to or diffuses through the protein pore, it affects the pore conductance by physically blocking the ion channel, thus, inducing a transient blockage in the ionic current (resistive pulse).[1,6,8,19,22] The nature of these transient blockages (e.g., magnitude, duration, and frequency) lead to molecular level discrimination, where the blockage magnitude and duration can elucidate the molecule identity, and frequency of the binding events correlates to the analyte concentration.[1,3]

Biological nanopore-based techniques necessitate a stable lipid bilayer to employ ion channels as a sensing element. The formation of an artificial lipid membrane can be achieved by conventional methods such as the painting method[23,24] and folding method,[25,26] by using microfabricated devices,[27] or by droplet-based techniques such as droplet-contact method,[28–30] droplet interface bilayer,[31,32] and droplet transfer method.[33] Although these methods were successfully applied to form lipid bilayers, some techniques, such as droplet-based methods, require specific tools or fabrication of microdevices. In addition, the conventional methods are limited to the fragility of unsupported (substrate-pore spanning) bilayers in conventional methods.[27,34,35] On the other hand, the tip-dip method, where the lipid membrane is formed at the glass probe end, is considered a facile method to form a stable bilayer without complicated devices or tools.[27] Moreover, this method allows for the integration of biological nanopores at the probe tip, which can be exploited not only in nanopore sensing applications but also for chemical imaging purposes such as scanning ion conductance microscopy (SICM).

The use of biological nanopores incorporated into SICM promises to bring the advantageous attributes of nanopore sensing to the spatial resolution and chemical imaging

functionality of SICM. To achieve this, glass micro-pipets are typically employed to support the lipid bilayer for SICM measurements.[21,36] Previous studies reported the use of glass pipet-supported ion channels either as a single barrel or dual barrel probe to monitor the molecular or ion flux from a porous substrate.[10,21,36–38] In a similar approach, we recently developed a recessed-in-glass Ag/AgCl microelectrode, where the probe geometry creates a spanning lipid bilayer that spans a glass pore in which a Ag/AgCl is at the bottom of the pore.[5] However, the spatial resolution is still limited by micrometer scale probe size, similar to other glass pipette probes used for ion channel recordings or SICM measurements.[5,10,21,36]

An alternative approach to the spanning lipid bilayer method is the use of electrode supported bilayers, which have been developed and employed for sensing purposes based on ion channels.[27,39–41] Building off these supported bilayers, Okuno et al.[42,43] developed polyethylene glycol (PEG)-modified gold nanoelectrodes to support lipid bilayer for ion channel recordings. This type of gold nanoneedle showed great promise in sensing applications and, more recently, in the ease of unzipping and reforming the lipid bilayer throughout the measurement time.[43–45] We recently demonstrated the utility of gold nanoneedle-probe-supported protein channels in the chemical detection of β-cyclodextrin (β-CD) with high spatial resolution in addition to their analysis method of protein de-insertion current for different types of pore-forming proteins.[44,45] Although the gold nanoneedle platform was applied as a nanopore sensor, it exhibits a significant channel current decay, ascribed to the double layer charging at the gold electrode surface. This observation consequently limits the long-term application of the gold as a support.

In this article, we introduce, for the first time, the use of silver nanoneedle to support lipid bilayer for ion channel measurement and single-molecule detection (Fig.1). Our findings propose the formation of an AgCl layer around the silver tip prepared in a chloride-containing etchant solution. In addition, we measure the channel current of alpha-hemolysin (αHL) protein pore reconstituted in the lipid bilayer formed at the silver tip. The resulting Ag/AgCl nanoneedle-supported biological nanopore represents a first of its kind probe that mitigates the challenges with working with similar probe geometries on non-polarizable electrode materials like gold. More specifically, the use of Ag/AgCl probes mitigates the unavoidable current decay observed when using gold nanoneedles which is a result of double layer charging that carries current at this electrode interface. The new nanoneedle probe describe here allows for more stable, sustained DC channel current recordings rendering the probe well-suited for translatable use in a broad range of analytical applications utilizing protein channels. Moreover, the ion channel probe is readily fabricated using benchtop methods making it accessible to a range of research groups. To

demonstrate utility of the new probe, we employed the silver nanoneedle-supported ion channel probe for nanopore sensing of sulfonated β-cyclodextrin (S_7βCD).

MATERIALS AND METHODS

Chemicals and Reagents

A 250μm diameter silver of 99.99% purity (Alfa Aesar) wire was utilized to fabricate silver nanoneedle. Perchloric acid (70% $HClO_4$; Sigma-Aldrich) and Methanol (HPLC grade; Sigma-Aldrich) were used in a 1:4 solution mixture for electrochemical etching of silver wire. Another etchant solution was prepared from 2M nitric acid (HNO_3; Fischer Chemical) and ethanol (ACS-USP grade; Decon labs). O-(3-carboxypropyl)-O′-[2-(3-mercaptopropionylamino)ethyl] propylethylene glycol (MW 3000; Sigma-Aldrich) and O-(2-Carboxyethyl)polyethylene glycol(MW 3,000; Sigma-Aldrich) were used as thiol-PEG and non-thiolated PEG, respectively. Thiol desorption experiments were performed in potassium hydroxide solution (KOH; Fischer Scientific). An electrolyte/buffer solution was made of potassium chloride (KCl; Sigma-Aldrich) or potassium nitrate (KNO_3; Sigma-Aldrich) in a sodium phosphate buffer (pH 7.4) composed of sodium dihydrogen phosphate ($NaH_2PO_4 \cdot 2H_2O$; Sigma-Aldrich) and disodium phosphate (Na_2HPO_4). The buffer solution was prepared using ultrapure water from a Milli-Q (Merck Millipore Corp.) resisted 18.2 MΩ at 25 °C. 1,2-Diphytanoyl-sn-glycero-3-phosphocholine (DPhPC; Avanti Polar Lipid) and n-decane (Merck Millipore Corp.) were used as the lipid/oil solution. Alpha-hemolysin (αHL; Sigma-Aldrich) isolated from *Staphylococcus aureus* was purchased as a monomer protein powder. Heptakis(6-O-sulfo)-β-cyclodextrin heptasodium salt (S_7βCD; Sigma-Aldrich) was used as the target analyte for single-molecule detection.

Fabrication and Characterization of Silver Nanoneedles

A silver nanoneedle was fabricated by electrochemical etching of silver microwire in a methanolic solution of perchloric acid ($HClO_4$:CH_3OH, 1:4).[46] 1-2 mm tip of silver wire was immersed in the etchant solution and a micro-positioner (Newport ULTRAlign 461-XYZ) was used to hold the silver wire vertically. Then, a DC voltage of 1V was applied between the silver microwire and a carbon rod counter electrode (2mm diameter). The etching process was complete when the current dropped to zero, typically within 4-5 minutes, indicating the silver wire was no longer in contact with the solution. The etched wire with a cone-shaped tip (silver nanoneedle) was then rinsed with deionized water (80˚C) and acetone before characterization. Two experiments using different conditions were performed to investigate the role chloride may be playing in the DC currents we observed; etching silver in non-chloride etchant of nitric acid in ethanol solution (HNO_3:

C_2H_5OH; 1:2) and the second was done by immersion of perchloric acid etched silver in a sodium hypochlorite solution (8.25%) to chloridate the wire, forming Ag/AgCl at the surface. Afterward, the silver tip surface was modified by immersion in a 60 mg/mL thiol-PEG solution in ethanol for 3h at room temperature and subsequently rinsed with ethanol and deionized water.[44] Scanning electron microscopy (Apreo SEM) operated at a voltage of 15kV was employed to characterize the morphology of the fabricated silver nanoneedles. The surface elemental composition was determined by an X-ray photoelectron spectroscope (XPS) equipped with both Al and Al-Mg dual-core in addition to a helium UV source.

Formation of a Lipid Membrane

The lipid bilayer was formed at the silver nanoneedle tip via the tip-dip method.[27,42,43] Briefly, a chamber was prepared by adding a buffered 1M KCl electrolyte aqueous phase in the bottom and a lipid/oil mixture (10mg/mL 1,2-Diphytanoyl-sn-glycero-3-phosphocholine solution in n-decane) at the top. In this arrangement, a lipid monolayer was formed at the interface between the lipid/oil mixture and the electrolyte bath in the chamber. The thiol PEG-modified silver was first soaked in electrolyte solution for few minutes so that an aqueous layer is formed around the tip. Afterwards, silver tip was dipped in the lipid/oil mixture and the aqueous layer around the tip acts as a support for a lipid monolayer. Two monolayers were merged to form a lipid bilayer at the silver tip when immersed across the oil-water interface via a micro-positioner (Newport ULTRAlign 461-XYZ).

Channel Current Recordings of Biological Nanopores

We used αHL protein prepared in 1MKCl/sodium phosphate buffer solution (pH 7.4) at a concentration of 30nM for channel current recordings. A potential of +100mV was applied between the silver nanoneedle and a quasi-reference-counter electrode (Ag/AgCl) inserted in the bath chamber. Prior to channel current recordings, the thiol PEG-modified silver nanoneedle was immersed in the electrolyte solution for 10 min to form an aqueous layer around the tip. We used two additional silver probes as controls; the first one was dipped in 60mg/mL non-thiolated PEG instead of thiol-PEG for 3h, and the second was used without surface modification before immersion in the electrolyte solution. Channel currents were monitored using a patch-clamp amplifier (PICO 2, Tecella) with a 7.9 kHz low-pass filter at a sampling frequency of 40kHz. Analysis of channel current was performed using pCLAMP version 10.7 (Molecular Devices).

Detection of S_7βCD and Data Analysis

To employ the fabricated silver probes in resistive pulse nanopore sensing, S_7βCD was added as a target analyte in the bath chamber (*trans* side). We used the thiol-PEG modified silver nanoneedle with αHL protein monomers added in the tip side solution (*cis* side). In this configuration, the heptameric αHL protein can be reconstituted from the tip side and S_7βCD binds to the protein pore from the *trans* side when a potential of +100mV was applied. To enhance the capture rate of binding events,[4] we applied an asymmetric salt gradient of 2M/ 0.5M KCl (*trans*/ *cis*). Channel current data and binding events in an αHL single channel were analyzed using pCLAMP 10.7 and correlated to the concentration of S_7βCD.

RESULTS AND DISCUSSION

Metal nanoneedle-supported ion channel probes have been recently developed to provide a nanopore sensing platform with high spatial resolution.[42,43] Expanding on the application of gold nanoneedle probes for single-molecule detection, Shoji et al.[44] successfully applied the gold nanoneedle-based ion channel probes for the chemical detection of sulfonated β-cyclodextrin (S_7βCD) with high spatial resolution. However, in all the previous reports, the gold probes exhibited an open channel current decay as well as a significant decrease in the binding events of S_7βCD to αHL pore throughout recording time.[44] The decrease in current is attributed to double layer charging at the gold electrode interface which carries the current at that working electrode. While this decay can be mitigated using asymmetric salt conditions across the lipid bilayer, it is problematic for practical applications of the probe. In this paper, we demonstrate the use of silver nanoneedle-supported lipid bilayers and biological nanopores in resistive pulse sensing (Fig.1). We compare the open channel current resulting from the silver nanoneedle to that of the gold nanoneedle based on previously published work[44] as well as our own comparison described in detail below.

Fabrication and Characterization of Silver Nanoneedles

We followed the electrochemical etching protocol for preparing silver tips used in scanning tunneling microscopy[46,47] to fabricate silver nanoneedles with a cone-shaped tip with an average diameter of 425 ± 33nm (Fig.2, top panel). The average tip diameter was measured from high-resolution SEM images for six perchloric acid-etched silver probes[48,49] (Fig.S1). In addition, other silver probes were fabricated in different conditions; the first was silver etched in the non-chloride etchant solution (2M nitric acid: ethanol, 1:2) and the other was a bleached silver probe after being etched in perchloric acid solution (Fig.2, top panel). As a result of varying the electrochemical

etching conditions, a variation in the produced tip geometry was observed where the average tip diameter for nitric acid-etched silver nanoneedles was 1.41 ± 0.08 μm, ~ 3 folds higher than the perchloric acid-etched probes. The SEM micrograph for the bleached silver probes showed a different surface morphology (Fig.2, top panel) due to the higher content of AgCl formed on the silver surface, similar to previous reports.[50–54]

We hypothesized that the silver surface is oxidized to silver chloride (AgCl) during the electrochemical etching procedure when performed in a chloride ion-containing solution such as perchloric acid and applying a DC voltage of 1V. Gray and Unwin[55] fabricated silver tips with similar conditions of anodic oxidation in 1M KCl solution and applied a potential of 0.2V. To understand the surface chemistry of the fabricated silver probes, we performed X-ray photoelectron spectroscopy (XPS) to elucidate the elemental composition at the surface. Fig.2 (bottom panel) and Fig.S2 show the high-resolution XPS spectra of Ag 3d and Cl 2p for the three silver nanoneedles prepared in different conditions. The peaks of Ag 3d in Fig.S2, inherent to the silver wire, clearly appeared at a binding energy of 367.9eV and 373.9eV and were assigned to Ag $3d_{5/2}$ and Ag $3d_{3/2}$, respectively for all probes. However, the Cl 2p peaks (Fig.2) were seen only on the perchloric acid-etched probe and bleached silver at a binding energy of 197.6eV and 199.2eV for $2p_{3/2}$ and $2p_{1/2}$, respectively. These results indicate that AgCl is likely formed during the etching of the probe. To further test our hypothesis of the presence of chloride, we calibrated the perchloric acid-etched silver nanoneedles in solutions of different chloride activity and recorded the open circuit potential (OCP).[55,56] The probes exhibited Nernstian behavior in a chloride concentration range of 10^{-5} to 10^{-1}M with a correlation factor (R^2) of 0.996 and a gradient of ~50 mV, in good agreement literature values[55–58] (Fig.S3).

Ag nanoneedle surface modification and formation of a Lipid Membrane

To investigate the role of silver nanoneedle surface modification with thiol PEG in supporting protein channel measurements, we performed control experiments using non-thiol PEG (MW 3000) and without PEG for both tip-side insertion and bath-side insertion. Our findings revealed that the pore conductance and current stability of the αHL protein channels are affected by different surface preparations, especially in the tip-side insertion configuration. The silver probes modified with non-thiol PEG or without PEG showed reduced pore conductance and unstable channel current in the tip-side insertion configuration (Fig.S4). Contrarily, the nanoneedles modified with thiol PEG exhibited stable current in both tip and bath insertion (Fig.S4).

Surface modification with thiol-PEG (Mw 3000) plays a key role to maintain αHL pore conductance as well as its performance in nanopore sensing, especially when αHL is inserted form tip-side. This is explained by the monolayer length (~24 nm) of thiol-PEG, which provides enough volume for the heptameric αHL structure (~10.5 nm length) to be reconstituted in the lipid bilayer from tip-side.[59–61] In terms of sensing application, the orientation of αHL into the lipid bilayer should be considered because some target analytes can easily translocate through αHL pore from *cis* side, such as ssDNA and RNA, while other analytes such as βCD can bind only to αHL from the *trans* side. In the latter case, αHL should be inserted from tip-side while βCD molecules are added to the bath side chamber. Thus, the surface modification of metal nanoneedle with thiol-PEG is crucial to employ αHL as a nanopore sensor. On the other hand, the absence of the PEG monolayer would provide a small aqueous layer (0.6-3 nm thick) around the silver tip.[62] Such conditions are suitable only for protein insertion from bath side with similar pore conductance regardless of surface modification (Fig S4).

To understand the way that thiol PEG is attached to silver nanoneedle, we used linear sweep voltammetry (LSV) to probe the reductive desorption of Ag-thiol bonds electrochemically. Earlier studies reported the electrochemical desorption of thiolate from Ag electrodes at negative potentials from -0.8V to -1.1V.[63–67] We performed the reductive desorption experiments in 0.1M KOH (pH=13) for perchloric acid-etched and nitric acid-etched silver nanoneedle. Both perchloric acid-etched and nitric acid-etched silver showed a thiol desorption peak around -0.85V (vs. Ag/AgCl) (Fig.3 and Fig.S5). This cathodic peak reduces in intensity with successive sweeps as shown in Fig.3, Fig.S5 and Fig.S6. These findings reveal the reductive desorption of thiolate from the silver nanoneedle indicating that thiol PEG has been chemisorbed on the silver surface.[65] However, we do not fully understand if the thiol PEG reduces some of the AgCl existing in the perchloric-etched silver probes to Ag or if the probe surface is comprised some chloride-free areas (bare Ag) to bind to the -SH group. This is under further investigation.

After surface modification of silver nanoneedle with thiol PEG, we formed an artificial lipid membrane via tip-dip method[27,42–44] using the DPhPC/n-decane as a lipid/oil mixture. The thiol PEG layer attached to the silver nanoneedle surface acts as a support for the aqueous solution around the silver tip. In this arrangement, two lipid monolayers are merged as previously described.[42–44] The lipid bilayer was successfully formed at the silver nanoneedle tip with a membrane capacitance of 0.42μF/cm^2 in agreement with reports for DPhPC.[68–70]

Channel Current Recordings of Biological Nanopores

When a stable lipid bilayer was formed, αHL was reconstituted into the lipid membrane. The protein insertion into the lipid bilayer was indicated by a step-like current increase[14] as the transmembrane protein pore allowed for free ion movement. The αHL pore produced a conductance of 1.19 ± 0.23 nS in 1M KCl symmetric solution conditions, similar to previous reports[5] (Fig.4). In addition, in contrast to the current-time traces on Au nanoneedles, the current-time traces in Fig.4 indicate a stable open channel current over time. Fig.5 shows a comparison between the current-time traces and the average normalized current for gold and silver nanoneedle-based ion channel probes over the time scale of 15s and 60s, respectively. It is clearly seen the channel current produced from the gold nanoneedle exhibited an exponential decay as previously reported by Shoji et al.[44] due to double layer charging at the electrode surface. The silver-based ion channel probes resulted in a more stable current over time as shown in Fig.4 and Fig.5. We assume the stable current observed with the silver probe is due to the formation of a layer of AgCl around the silver nanoneedle tip during etching. The resulting Ag/AgCl nanoneedle can act as an ideally non-polarizable electrode. More interestingly, we recorded the open channel current for silver nanoneedles prepared in different conditions; the nitric acid-etched and the bleached silver. As demonstrated in Fig.S7, both perchloric acid-etched and bleached silver probes similarly produced a stable current due to the chloride content in the surface, while the silver probe prepared in a chloride-free medium (nitric acid-etched) led to a current decay (Fig.S7). These results are in agreement with our surface characterization results that revealed the presence of chloride on the perchloric acid-etched and bleached silver probes and not on the nitric acid-etched probe (Fig.2 and Fig.S3).

Detection of S_7βCD and Data Analysis

To employ the silver nanoneedle-based ion channel probe in resistive pulse sensing, we detected the binding events of S_7βCD molecules using αHL pore. As S_7βCD molecules can access their binding sites in αHL pore from *trans* side only,[61] we added S_7βCD in bath solution and αHL protein solution was present in the tip-side solution at a concentration of 10nM. The potential applied across the lipid membrane will produce an electric field around the pore which is the driving force for the molecules to arrive at the pore.[4] The effect of applying salt gradient across the pore has been reported, where the asymmetric salt profiles increase the electric field around the pore resulting in enhancing the capture rate of target molecule as well as the blocking current magnitude[4,71–74] (Fig.S8). To enhance the rate of βCD binding to αHL, we used an asymmetric salt condition of 2M/0.5M KCl (*trans*/*cis*) along with applying 100mV. The binding events of S_7βCD were observed and correlated to concentrations. Fig.6 shows the number of blocking events due

to S_7βCD binding to αHL pore increased with higher concentrations. The relationship between binding frequency and S_7βCD concentration was linearly fit (R^2=0.999; n=4) in the concentration range from 1μM to 100μM. We also analyzed the dwell time and %blocking current for 632 binding events where the median current blocking percentage and dwell time were 81.2% and 10 ms, respectively (Fig.6). These results demonstrate the feasibility of our new silver nanoneedle-based ion channel probe platform as a resistive pulse nanopore sensor.

CONCLUSIONS

In conclusion, we described the synthesis of silver nanoneedle by electrochemical etching of silver microwire in perchloric acid solution. Characterization and electrochemical methods were accomplished to understand the surface chemistry of the silver probes before and after modification with thiol PEG. The obtained results suggested the formation of Ag/AgCl surface which led to DC stable channel current. The newly described (and first of its kind) silver nanoneedle with AgCl does represent a novel method that overcomes the major hurdle, channel current decay, when employing polarizable electrodes (gold) as supports. We successfully formed a lipid membrane at the silver tip and recorded the channel current using αHL protein pore. Finally, we applied these probes for single molecule detection of S_7βCD as a target analyte in the concentration range from 1 to 100 μM. Future advances to this silver nanoneedle platform will include the ability to maintain single channel for long term measurements. This will enable the use of the silver nanoneedles as a bio-SICM tool to monitor molecular flux from different substrates.

ACKNOWLEDGEMENTS

This material is based upon the work supported by the National Science Foundation (CHE 1608679 and CHE 2108368). The table of contents figure and figure 1 created with BioRender.com.

SUPPORTING INFORMATION

Evaluation of silver tip diameter, XPS spectra, calibration curve of potentiometric response experiment, effect of surface modification on pore conductance, linear sweep voltammograms, Integrated thiol desorption peak areas, recorded channel current for different tips, and event frequencies using different salt conditions.

REFERENCES

(1) Bayley, H.; Martin, C. R. Resistive-Pulse Sensing - from Microbes to Molecules. *Chem. Rev.* **2000**, *100*, 2575–2594.

(2) Kozak, D.; Anderson, W.; Vogel, R.; Trau, M. Advances in Resistive Pulse Sensors: Devices Bridging the Void between Molecular and Microscopic Detection. *Nano Today* **2011**, *6*, 531–545.

(3) Pan, R.; Hu, K.; Jiang, D.; Samuni, U.; Mirkin, M. V. Electrochemical Resistive-Pulse Sensing. *J. Am. Chem. Soc.* **2020**, *141*, 19555–19559.

(4) Wanunu, M.; Morrison, W.; Rabin, Y.; Grosberg, A. Y.; Meller, A. Electrostatic Focusing of Unlabelled DNA into Nanoscale Pores Using a Salt Gradient. *Nat. Nanotechnol.* **2010**, *5*, 160–165.

(5) Shoji, K.; Kawano, R.; White, R. J. Recessed Ag/AgCl Microelectrode-Supported Lipid Bilayer for Nanopore Sensing. *Anal. Chem.* **2020**, *92*, 10856–10862.

(6) Wang, Y.; Zheng, D.; Tan, Q.; Wang, M. X.; Gu, L. Q. Nanopore-Based Detection of Circulating MicroRNAs in Lung Cancer Patients. *Nat. Nanotechnol.* **2011**, *6*, 668–674.

(7) Zhang, X.; Wang, Y.; Fricke, B. L.; Gu, L. Q. Programming Nanopore Ion Flow for Encoded Multiplex MicroRNA Detection. *ACS Nano* **2014**, *8*, 3444–3450.

(8) Akeson, M.; Branton, D.; Kasianowicz, J. J.; Brandin, E.; Deamer, D. W. Microsecond Time-Scale Discrimination among Polycytidylic Acid, Polyadenylic Acid, and Polyuridylic Acid as Homopolymers or as Segments within Single RNA Molecules. *Biophys. J.* **1999**, *77*, 3227–3233.

(9) Boersma, A. J.; Brain, K. L.; Bayley, H. Real-Time Stochastic Detection of Multiple Neurotransmitters with a Protein Nanopore. *ACS Nano* **2012**, *6* , 5304–5308.

(10) MacAzo, F. C.; White, R. J. Monitoring Charge Flux to Quantify Unusual Ligand-Induced Ion Channel Activity for Use in Biological Nanopore-Based Sensors. *Anal. Chem.* **2014**, *86*, 5519–5525.

(11) Boersma, A. J.; Bayley, H. Continuous Stochastic Detection of Amino Acid Enantiomers with a Protein Nanopore. *Angew. Chemie* **2012**, *124*, 9744–9747.

(12) Piguet, F.; Ouldali, H.; Pastoriza-Gallego, M.; Manivet, P.; Pelta, J.; Oukhaled, A. Identification of Single Amino Acid Differences in Uniformly Charged Homopolymeric Peptides with Aerolysin Nanopore. *Nat. Commun.* **2018**, *9*, 1-13.

(13) Kowalczyk, S. W.; Hall, A. R.; Dekker, C. Detection of Local Protein Structures along DNA Using Solid-State Nanopores. *Nano Lett.* **2010**, *10*, 324–328.

(14) Watanabe, H.; Gubbiotti, A.; Chinappi, M.; Takai, N.; Tanaka, K.; Tsumoto, K.; Kawano, R. Analysis of Pore Formation and Protein Translocation Using Large Biological Nanopores. *Anal. Chem.* **2017**, *89*, 11269–11277.

(15) Clarke, J.; Wu, H. C.; Jayasinghe, L.; Patel, A.; Reid, S.; Bayley, H. Continuous Base Identification for Single-Molecule Nanopore DNA Sequencing. *Nat. Nanotechnol.* **2009**, *4*, 265–270.

(16) Venkatesan, B. M.; Bashir, R. Nanopore Sensors for Nucleic Acid Analysis. *Nat. Nanotechnol.* **2011**, *6*, 615–624.

(17) Varongchayakul, N.; Song, J.; Meller, A.; Grinstaff, M. W. Single-Molecule Protein Sensing in a Nanopore: A Tutorial. *Chem. Soc. Rev.* **2018**, *47*, 8512–8524.

(18) Hall, A. R.; Scott, A.; Rotem, D.; Mehta, K. K; Bayley, H.; Dekker, C. Hybrid Pore Formation by Directed Insertion of Alpha Hemolysin into Solid-State Nanopores. *Bone* **2012**, *23* , 1–7.

(19) Shi, W.; Friedman, A. K.; Baker, L. A. Nanopore Sensing. *Anal. Chem.* **2017**, *89* , 157–188..

(20) Song, Y.; Zhang, J.; Li, D. Microfluidic and Nanofluidic Resistive Pulse Sensing: A Review. *Micromachines* **2017**, *8* , 1–19..

(21) Macazo, F. C.; White, R. J. Bioinspired Protein Channel-Based Scanning Ion Conductance Microscopy (Bio-SICM) for Simultaneous Conductance and Specific Molecular Imaging. *J. Am. Chem. Soc.* **2016**, *138*, 2793–2801.

(22) Lazenby, R. A.; Macazo, F. C.; Wormsbecher, R. F.; White, R. J. Quantitative Framework for Stochastic Nanopore Sensors Using Multiple Channels. *Anal. Chem.* **2018**, *90*, 903–911..

(23) Mueller,P.; Rudin, D. O.; Ti Tien, H.; Wescott, W. C. Reconstitution of Cell Membrane Structure in Vitro and Its Transformation into an Excitable System. *Nature* **1962**, *194*, 979–980.

(24) Derrington, I. M.; Butler, T. Z.; Collins, M. D.; Manrao, E.; Pavlenok, M.; Niederweis, M.; Gundlach, J. H. Nanopore DNA Sequencing with MspA. *Proc. Natl. Acad. Sci. U. S. A.* **2010**, *107*, 16060–16065.

(25) Montal, M.; Mueller, P. Formation of Bimolecular Membranes from Lipid Monolayers and a Study of Their Electrical Properties. *Proc. Natl. Acad. Sci. U. S. A.* **1972**, *69*, 3561–3566.

(26) M. Sugawara, A. H. *Advances in Planar Lipid Bilayers and Liposomes*; Elsevier Amsterdam, The Netherlands, **2005**.

(27) Hirano-Iwata, A.; Niwano, M.; Sugawara, M. The Design of Molecular Sensing Interfaces with Lipid-Bilayer Assemblies. *TrAC - Trends Anal. Chem.* **2008**, *27*, 512–520.

(28) Kawano, R.; Tsuji, Y.; Sato, K.; Osaki, T.; Kamiya, K.; Hirano, M.; Ide, T.; Miki, N.; Takeuchi, S. Automated Parallel Recordings of Topologically Identified Single Ion Channels. *Sci. Rep.* **2013**, *3*, 1–7.

(29) Funakoshi, K.; Suzuki, H.; Takeuchi, S. Lipid Bilayer Formation by Contacting Monolayers in a Microfluidic Device for Membrane Protein Analysis. *Anal. Chem.* **2006**, *78*, 8169–8174.

(30) Shoji, K.; Kawano, R. Microfluidic Formation of Double-Stacked Planar Bilayer Lipid Membranes by Controlling the Water-Oil Interface. *Micromachines* **2018**, *9*.

(31) Bayley, H.; Cronin, B.; Heron, A.; Holden, M. A.; Hwang, W. L.; Syeda, R.; Thompson, J.; Wallace, M. Droplet Interface Bilayers. *Mol. BioSyst.* **2008**, *4*, 1191–1208.

(32) Hwang, W. L.; Holden, M. A.; White, S.; Bayley, H. Electrical Behavior of Droplet Interface Bilayer Networks: Experimental Analysis and Modeling. *J. Am. Chem. Soc.* **2007**, *129*, 11854–11864.

(33) Yanagisawa, M.; Iwamoto, M.; Kato, A.; Yoshikawa, K.; Oiki, S. Oriented Reconstitution of a Membrane Protein in a Giant Unilamellar Vesicle: Experimental Verification with the Potassium Channel KcsA. *J. Am. Chem. Soc.* **2011**, *133*, 11774–11779.

(34) White, R. J.; Ervin, E. N.; Yang, T.; Chen, X.; Daniel, S.; Cremer, P. S.; White, H. S. Single Ion-Channel Recordings Using Glass Nanopore Membranes. *J. Am. Chem. Soc.* **2007**, *129*, 11766–11775.

(35) A. Ottova, H. T. T. *Advances in Planar Lipid Bilayers and Liposomes*; Elsevier, **2005**.

(36) Zhou, Y.; Bright, L. K.; Shi, W.; Aspinwall, C. A.; Baker, L. A. Ion Channel Probes for Scanning Ion Conductance Microscopy. *Langmuir* **2014**, *30*, 15351–15355.

(37) Shi, W.; Zeng, Y.; Zhou, L.; Xiao, Y.; Cummins, T. R.; Baker, L. A. Membrane Patches as Ion Channel Probes for Scanning Ion Conductance Microscopy. *Faraday Discuss.* **2016**, *193*, 81–97.

(38) Shi, W.; Zeng, Y.; Zhu, C.; Xiao, Y.; Cummins, T. R.; Hou, J.; Baker, L. A. Characterization of Membrane Patch-Ion Channel Probes for Scanning Ion Conductance Microscopy. *Small* **2018**, *14*, 1–10.

(39) Richter, R. P.; Bérat, R.; Brisson, A. R. Formation of Solid-Supported Lipid Bilayers: An Integrated View. *Langmuir* **2006**, *22*, 3497–3505.

(40) Tien, H. T.; Ottova, A. L. Supported Planar Lipid Bilayers (s-BLMs) as Electrochemical Biosensors. *Electrochim. Acta* **1998**, *43*, 3587–3610.

(41) Naumann, R.; Jonczyk, A.; Kopp, R.; van Esch, J.; Ringsdorf, H.; Knoll, W.; Gräber, P. Incorporation of Membrane Proteins in Solid-Supported Lipid Layers. *Angew. Chemie Int. Ed. English* **1995**, *34*, 2056–2058.

(42) Okuno, D.; Hirano, M.; Yokota, H.; Onishi, Y.; Ichinose, J.; Ide, T. A Simple Method for Ion Channel Recordings Using Fine Gold Electrode. *Anal. Sci.* **2016**, *32*, 1353–1357.

(43) Okuno, D.; Hirano, M.; Yokota, H.; Ichinose, J.; Kira, T.; Hijiya, T.; Uozumi, C.; Yamakami, M.; Ide, T. A Gold Nano-Electrode for Single Ion Channel Recordings. *Nanoscale* **2018**, *10*, 4036–4040..

(44) Shoji, K.; Kawano, R.; White, R. J. Spatially Resolved Chemical Detection with a Nanoneedle-Probe-Supported Biological Nanopore. *ACS Nano* **2019**, 13, 2606-2614.

(45) Shoji, K.; Kawano, R.; White, R. J. Analysis of Membrane Protein Deinsertion-Associated Currents with Nanoneedle-Supported Bilayers to Discover Pore Formation Mechanisms. *Langmuir* **2020**, *36*, 10012–10021.

(46) Zhang, C.; Gao, B.; Chen, L. G.; Meng, Q. S.; Yang, H.; Zhang, R.; Tao, X.; Gao, H. Y.; Liao, Y.; Dong, Z. C. Fabrication of Silver Tips for Scanning Tunneling Microscope Induced Luminescence. *Rev. Sci. Instrum.* **2011**, *82*, 1–5.

(47) Iwami, M.; Uehara, Y.; Ushioda, S. Preparation of Silver Tips for Scanning Tunneling Microscopy Imaging. *Rev. Sci. Instrum.* **1998**, *69*, 4010–4011.

(48) Huang, T. X.; Huang, S. C.; Li, M. H.; Zeng, Z. C.; Wang, X.; Ren, B. Tip-Enhanced Raman Spectroscopy: Tip-Related Issues. *Anal. Bioanal. Chem.* **2015**, *407*, 8177–8195.

(49) Yang, B.; Kazuma, E.; Yokota, Y.; Kim, Y. Fabrication of Sharp Gold Tips by Three-Electrode Electrochemical Etching with High Controllability and Reproducibility. *J. Phys. Chem. C* **2018**, *122*, 16950–16955.

(50) Pargar, F.; Koleva, D. A.; Copuroglu, O.; Koenders, E. A. B.; van Breugel, K. Evaluation of Ag/AgCl Sensors for in-Situ Monitoring of Freee Chloride Concentration in Reinforced

Concrete Structures. *Young Res. Forum II Constr. Mater.* **2014**, 153–158.

(51) Ziółkowski, R.; Górski, Ł.; Prokaryn, P.; Zaborowski, M.; Kutyła-Olesiuk, A.; Ciosek, P.; Wróblewski, W.; Malinowska, E. Development of Silicon-Based Electrochemical Transducers. *Anal. Methods* **2013**, *5*, 5464–5470.

(52) Brewer, P. J.; Brown, R. J. C. Effect of Silver Annealing Conditions on the Performance of Electrolytic Silver/Silver Chloride Electrodes Used in Harned Cell Measurements of PH. *Sensors* **2010**, *10*, 2202–2216..

(53) Safari, S.; Selvaganapathy, P. R.; Derardja, A.; Deen, M. J. Electrochemical Growth of High-Aspect Ratio Nanostructured Silver Chloride on Silver and Its Application to Miniaturized Reference Electrodes. *Nanotechnology* **2011**, *22*, 315601–315609.

(54) Kim, S.; Park, G.; Ahn, H. J.; Yoo, B. U.; Song, I. H.; Lee, K. H.; Kim, K. H.; Lim, J. H.; Lee, J. Y. Facial Fabrication and Characterization of Novel Ag/AgCl Chloride Ion Sensor Based on Gel-Type Electrolyte. *Front. Chem.* **2020**, *8*, 1–13.

(55) Gray, N. J.; Unwin, P. R. Simple Procedure for the Fabrication of Silver/Silver Chloride Potentiometric Electrodes with Micrometre and Smaller Dimensions: Application to Scanning Electrochemical Microscopy. *Analyst* **2000**, *125*, 889–893.

(56) Pargar, F.; Kolev, H.; Koleva, D. A.; Van Breugel, K. Potentiometric Response of Ag/AgCl Chloride Sensors in Model Alkaline Medium. *Adv. Mater. Sci. Eng.* **2018**, *2018*, 1–12.

(57) Elsener, B.; Zimmermann, L.; Böhni, H. Non Destructive Determination of the Free Chloride Content in Cement Based Materials. *Mater. Corros.* **2003**, *54*, 440–446.

(58) Montemor, M. F.; Alves, J. H.; Simões, A. M.; Fernandes, J. C. S.; Lourenço, Z.; Costa, A. J. S.; Appleton, A. J.; Ferreira, M. G. S. Multiprobe Chloride Sensor for in Situ Monitoring of Reinforced Concrete Structures. *Cem. Concr. Compos.* **2006**, *28*, 233–236.

(59) Furini, S.; Domene, C.; Rossi, M.; Tartagni, M.; Cavalcanti, S. Model-Based Prediction of the α-Hemolysin Structure in the Hexameric State. *Biophys. J.* **2008**, *95*, 2265–2274.

(60) Song, L.; Hobaugh, M. R.; Shustak, C.; Cheley, S.; Bayley, H.; Gouaux, J. E. Structure of Staphylococcal α-Hemolysin, a Heptameric Transmembrane Pore. *Science (80-.).* **1996**, *274*, 1859–1866.

(61) Gu, L. Q.; Bayley, H. Interaction of the Noncovalent Molecular Adapter, β-Cyclodextrin, with the Staphylococcal α-Hemolysin Pore. *Biophys. J.* **2000**, *79*, 1967–1975.

(62) White, R. J.; Zhang, B.; Daniel, S.; Tang, J. M.; Ervin, E. N.; Cremer, P. S.; White, H. S. Ionic Conductivity of the Aqueous Layer Separating a Lipid Bilayer Membrane and a Glass Support. *Langmuir* **2006**, *22*, 10777–10783.

(63) Matsuura, H.; Sato, Y.; Sawaguchi, T.; Mizutani, F. Highly Sensitive Determination of Acetylcholinesterase Activity Based on the Chemisorption/Reductive Desorption-Process of Thiol Compound on a Silver Electrode. *Chem. Lett.* **2002**, *1*, 618–619..

(64) Esplandiu, M. J.; Hagenstrom, H. Functionalized Self-Assembled Monolayers and Their Influence on Silver Electrodeposition. *Solid State Ionics* **2002**, *150*, 39–52.

(65) Mohtat, N.; Byloos, M.; Soucy, M.; Morin, S.; Morin, M. Electrochemical Evidence of the Adsorption of Alkanethiols on Two Sites on Ag(111). *J. Electroanal. Chem.* **2000**, *484*, 120–130..

(66) Hatchett, D. W.; Stevenson, K. J.; Lacy, W. B.; Harris, J. M.; White, H. S. Electrochemical Oxidative Adsorption of Ethanethiolate on Ag(111). *J. Am. Chem. Soc.* **1997**, *119*, 6596–6606.

(67) Hatchett, D. W.; Uibel, R. H.; Stevenson, K. J.; Harris, J. M.; White, H. S. Electrochemical Measurement of the Free Energy of Adsorption of N-Alkanethiolates at Ag(111). *J. Am. Chem. Soc.* **1998**, *120*, 1062–1069.

(68) Moellerfeld, J.; Prass, W.; Ringsdorf, H.; Hamazaki, H.; Sunamoto, J. Improved Stability of Black Lipid Membranes by Coating with Polysaccharide Derivatives Bearing Hydrophobic Anchor Groups. *BBA - Biomembr.* **1986**, *857*, 265–270.

(69) Gross, L. C. M.; Heron, A. J.; Baca, S. C.; Wallace, M. I. Determining Membrane Capacitance by Dynamic Control of Droplet Interface Bilayer Area. *Langmuir* **2011**, *27*, 14335–14342.

(70) Wang, J.; Benier, L.; Winterhalter, M. Quantifying Permeation of Small Charged Molecules across Channels: Electrophysiology in Small Volumes. *ACS Omega* **2018**, *3*, 17481–17486..

(71) Sha, J.; Shi, H.; Zhang, Y.; Chen, C.; Liu, L.; Chen, Y. Salt Gradient Improving Signal-to-Noise Ratio in Solid-State Nanopore. *ACS Sensors* **2017**, *2*, 506–512.

(72) Huang, G.; Willems, K.; Bartelds, M.; Van Dorpe, P.; Soskine, M.; Maglia, G. Electro-Osmotic Vortices Promote the Capture of Folded Proteins by Plyab Nanopores. *Nano Lett.* **2020**, *20*, 3819–3827..

(73) Nova, I. C.; Derrington, I. M.; Craig, J. M.; Noakes, M. T.; Tickman, B. I.; Doering, K.; Higinbotham, H.; Laszlo, A. H.; Gundlach, J. H. Investigating Asymmetric Salt Profiles for Nanopore DNA Sequencing with Biological Porin MspA. *PLoS One* **2017**, *12*, 1–14.

(74) Jeon, B. J.; Muthukumar, M. Polymer Capture by α-Hemolysin Pore upon Salt Concentration Gradient. *J. Chem. Phys.* **2014**, *140*, 1–7.

FIGURES

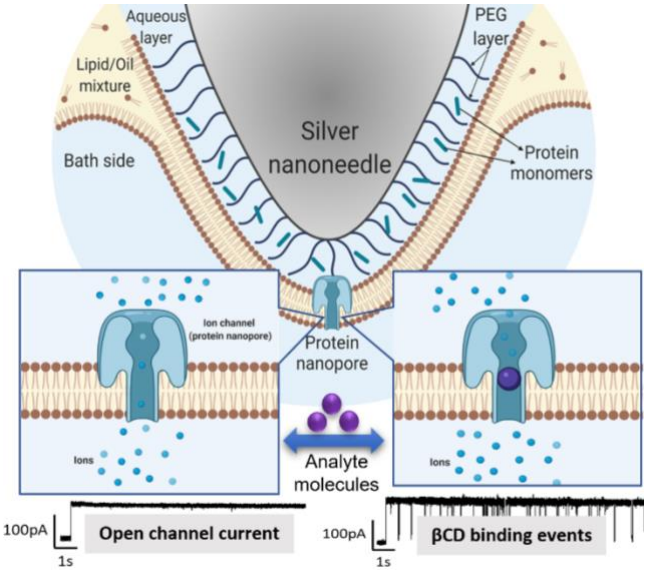

Figure 1. Schematic illustration of silver nanoneedle-based ion channel probe. The probe consists of electrochemically-etched silver wire with thiol-PEG surface modification. (Left) αHL inserts from the aqueous solution between the membrane and silver surface. (Right) S_7βCD molecules in the bath side bind to αHL protein pore resulting in resistive pulses.

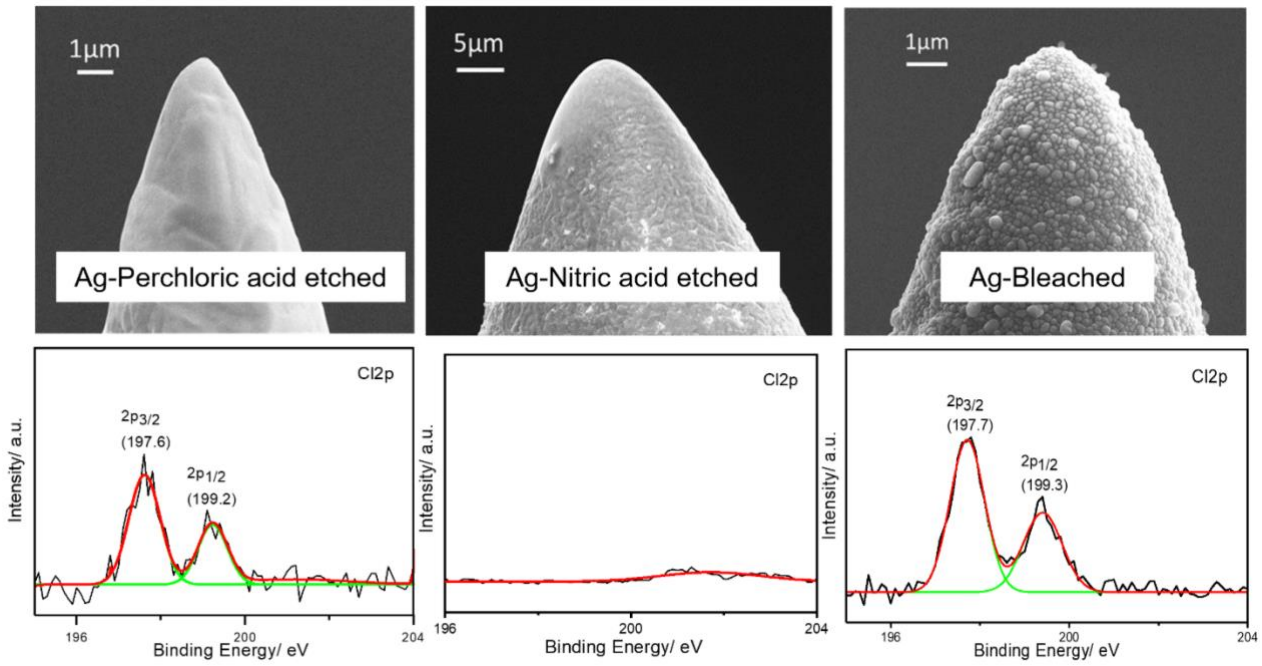

Figure 2. Surface characterization of silver nanoneedle probes prepared in different conditions. (Top panel) SEM micrographs for perchloric acid-etched, nitric acid-etched, and bleached silver, respectively from the left to the right. (Bottom) The corresponding HR-XPS spectra (Cl 2p) for the fabricated silver nanoneedles.

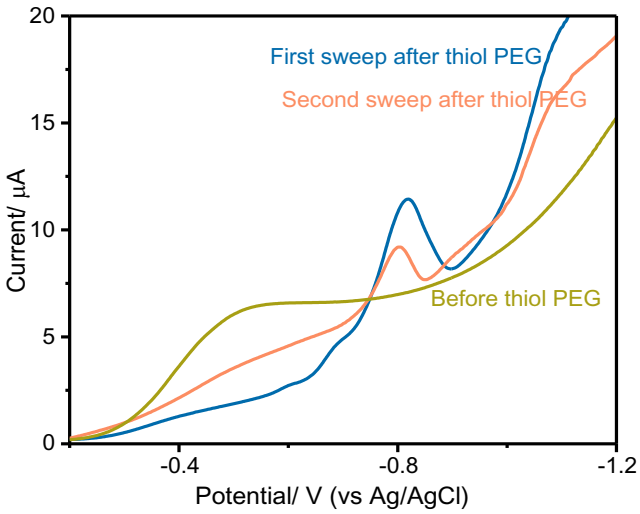

Figure 3. Linear sweep voltammograms for reductive desorption of thiol PEG from silver nanoneedle surface in 0.1M KOH (sweep rate: 50 mV/s). In this plot, cathodic currents are plotted as positive.

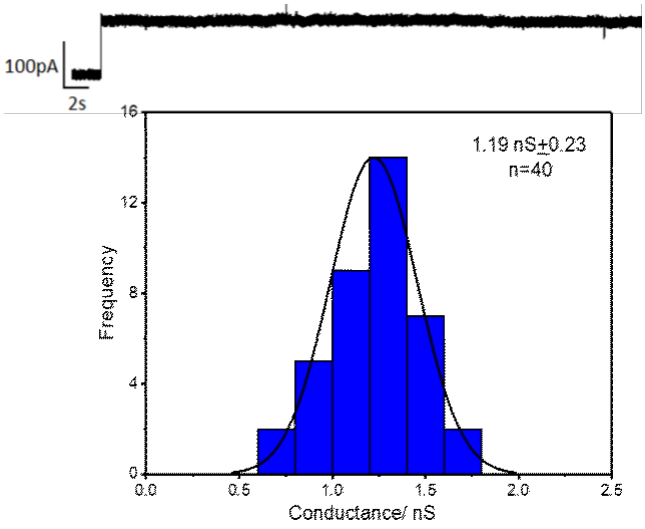

Figure 4. (Top) Open channel current for αHL nanopore in 1M KCl solution. (Bottom) Measured conductance for 40 αHL channels at a potential of 100mV. The mean pore conductance value was 1.19 ± 0.23 nS.

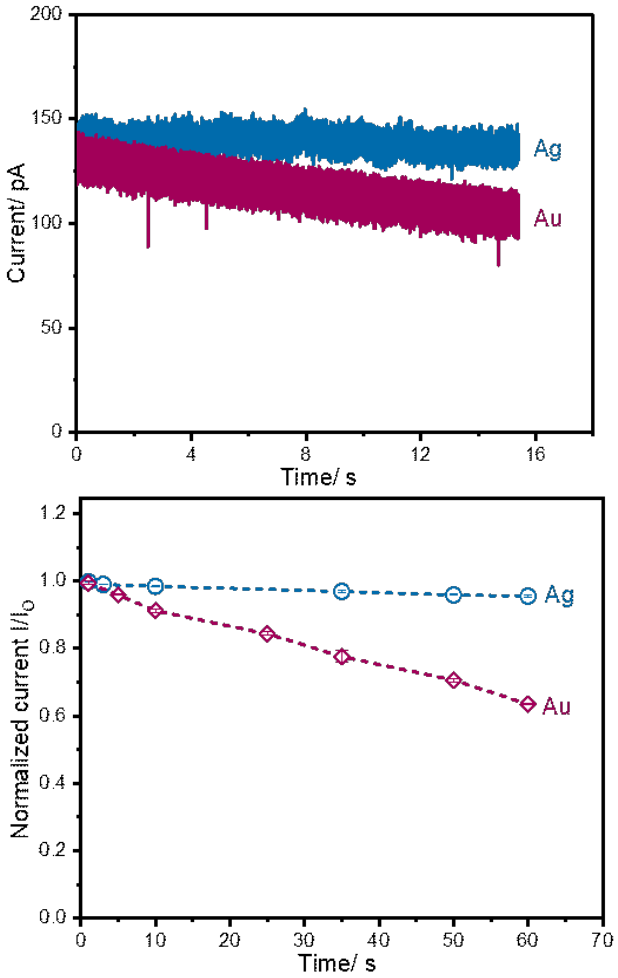

Figure 5. Channel current decay for silver nanoneedle compared to the gold nanoneedle. (Top) Current-time traces for αHL nanopore using both gold and silver nanoneedles. (Bottom) the average current produced over longer recording time where the channel current showed remarkable decay after 1 minute of recording.

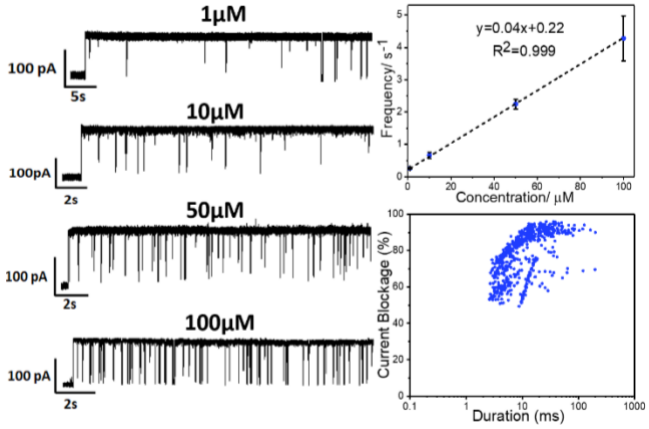

Figure 6. Single-molecule detection of βCD in the bath side solution. (Left) Frequency of βCD binding events is proportional to the concentration of βCD in the bath solution. (Top Right) Calibration curve of βCD shows the linear correlation between event frequency and βCD concentration of 1, 10, 50, and 100 μM. (Bottom Right) scatter plot of the current blockage and dwell time. The median dwell time for blocking events (78% average blockage) was 10ms.

For Table of Contents Only